

# Large planar topological Hall effect in a uniaxial van der Waals ferromagnet Fe<sub>3</sub>GeTe<sub>2</sub>

Yurong You<sup>1</sup>, Yuanyuan Gong<sup>1</sup>, Zefang Li<sup>2</sup>, Hang Li<sup>2</sup>, Mengmei Zhu<sup>1</sup>, Jiaxuan Tang<sup>1</sup>, Enke Liu<sup>2</sup>, Yuan Yao<sup>2</sup>, Guizhou Xu<sup>1,a</sup>, Feng Xu<sup>1,a</sup>, Wenhong Wang<sup>2</sup>

<sup>1</sup> School of Materials Science and Engineering, Nanjing University of Science and Technology, Nanjing 210094, China

<sup>2</sup> State Key Laboratory for Magnetism, Beijing National Laboratory for Condensed Matter Physics, Institute of Physics, Chinese Academy of Sciences, Beijing 100190, China

## Abstract

In this work, we reported the first observation of a large planar topological Hall effect (PTHE) in single crystal of Fe<sub>3</sub>GeTe<sub>2</sub>, a paradigm two-dimensional ferromagnet. The Hall effect and magnetoresistance varied systematically when the external magnetic field rotated in the *ac* (or *bc*) plane, where the PTHE emerged and maintained robust with field swept across the hard-magnetized *ab* plane. The PTHE covers the whole temperature region below T<sub>c</sub> (~150K) and reaches a maximum with  $\rho_{xy}^{PT}$  of 2.04  $\mu\Omega \cdot \text{cm}$  at 100K. Emergence of a nontrivial internal field was proposed to explain the origin of this large PTHE, which is either generated by the possible topological domain structure of uniaxial Fe<sub>3</sub>GeTe<sub>2</sub> or the non-coplanar spin structure formed during the in-plane magnetization. Our results promisingly provide an alternative detection method to the in-plane skyrmion formation and may bring brand-new prospective to magneto-transport studies in condensed matter physics.

---

a) Authors to whom correspondence should be addressed. E-mail: [gzxu@njust.edu.cn](mailto:gzxu@njust.edu.cn),  
[xufeng@njust.edu.cn](mailto:xufeng@njust.edu.cn)

## Introduction

Emergent electromagnetism<sup>1</sup> induced by the internal gauge field has triggered many novel and interesting transport phenomena, for instance, the unusual large anomalous Hall effect (AHE) in non-collinear antiferromagnets<sup>2-4</sup> or contributed by topological Weyl or nodal line band structure<sup>5,6</sup>. On the other hand, topological Hall effect (THE) is also uncovered in systems with scalar spin chirality<sup>7,8</sup> or topological spin texture<sup>9-11</sup> (skyrmions, typically). These Berry-phase driven phenomena have deeply enrich our understanding of the fundamental physics of magneto transport, especially the Hall effect, as well as offer versatile options to spintronic applications<sup>3,6</sup>.

A regular Hall effect is measured during the applied magnetic field ( $\mathbf{H}$ ), the electrical current ( $\mathbf{I}$ ) and the measured voltage ( $\mathbf{V}$ ) are mutually vertical. There exists a so-called planar Hall effect (PHE)<sup>12</sup>, where the Hall signal is otherwise obtained in the plane parallel to  $\mathbf{H}$ . PHE is resulted by neither of the mechanism account for AHE, but actually relates to the anisotropic magnetoresistance (AMR)<sup>13,14</sup>. Giant PHE has been reported in the ferromagnetic semiconductor films<sup>15</sup> and recently in the topological Weyl semimetal that correlates with chiral-anomaly<sup>16,17</sup>. However, the essence of PHE makes it exhibit symmetric curves while sweeping  $\mathbf{H}$ , as observed in most cases<sup>15,18</sup>, rather than antisymmetric one like a normal Hall effect. In addition, the transverse voltage will vanish when  $\mathbf{I}$  is perpendicular or parallel to  $\mathbf{H}$  according to its phenomenological expression (will be discussed later). But there are several works reported the AHE-like signal in a PHE configuration<sup>19,20</sup>, which are currently explained by either a high-order contribution or non-collinear spin structure.

Here we identified a novel planar topological Hall effect (PTHE) in a quasi-two dimensional van der Waals ferromagnet  $\text{Fe}_3\text{GeTe}_2$ <sup>21</sup>. The signal of THE gradually emerges when  $\mathbf{H}$  rotated away from its usual perpendicular direction, and reaches the maximum in the same  $ab$  plane where the Hall signal is measured. So, we named it as PTHE, to distinguish from the existed THE observed in a normal three-axis configuration. It should be noted that Yihao Wang *et al*<sup>22</sup> have already reported similar-shape THE in  $\text{Fe}_3\text{GeTe}_2$ , but they applied conventional configuration, which is different from the phenomenon observed here. Two assumptions are proposed for the origin of the observed large PTHE. Our results potentially provide an effective method to detect the in-plane topological spin texture, particular in 2D system and thin films, and further extend the understanding of the Hall

effect and bring new prospective to magnetotransport studies in condensed matter physics.

## Methods

High-quality single crystal samples were grown through the self-flux method<sup>23</sup> from a mixture of pure elements Fe (99.8%), Ge (99.9999%) and Te (99.99%) with a composition of Fe<sub>2</sub>GeTe<sub>4</sub>. The mixture was then sealed in an evacuated quartz tube and heated to 960°C. The melt was held at 960°C for 12h, then cooled slowly to 675°C with a rate of 3°C/h, and finally cooled down to room temperature. Typical size of the single crystals are  $\sim 2 \times 2 \times 0.1$ mm, with cleavable layer in the *ab* plane. The crystal structure was identified by X-ray diffraction (XRD, Bruker D8 Advance) with Cu-K $\alpha$  radiation. Element composition and atomic configuration were examined by energy-dispersive spectroscopy (EDS) in the scanning electron microscope (SEM, FEI Quanta 250F) and high-resolution scanning transmission electron microscopy (STEM), respectively. The atomic ratio determined by EDS is  $\sim 3: 1: 2.2$ , exhibiting slightly off-stoichiometric, which may account for the lowering Curie temperature of our sample comparing to the ones grown by the chemical vapor transport (CVT)<sup>24-26</sup>. Magnetization and transport properties were measured in the superconducting quantum interference device (SQUID) and physical property measurement system (PPMS, Quantum Design) respectively. For transport measurements, the samples were cut into standard Hall-bar shape slices and a six-probe method is applied to simultaneously measure the magnetoresistance (MR) and Hall resistivity  $\rho_{xy}$ . The MR and Hall data were symmetrized to exclude the misalignment of the electrode.

## Results and discussions

Fe<sub>3</sub>GeTe<sub>2</sub> is a van der Waals ferromagnet that crystallizes in space group *P6<sub>3</sub>/mmc* with a layered Fe<sub>3</sub>Ge substructure sandwiched by two Te layers<sup>21</sup>. As shown in Fig. 1(a), The Fe<sub>3</sub>Ge substructure contains two inequivalent FeI and FeII atoms, contributing to a FeII-Ge hexagonal atomic ring layer and two separated triangular lattice FeI-FeI layer. The hexagonal ring was clearly resolved in the high-resolution STEM image in Fig. 1(b), confirming the stacked structure and high quality of our samples. The X-ray diffraction in Fig. 1(c) verified the expected single crystalline nature of our sample, with all the reflections along the crystallographic orientation [001].

The temperature dependence of magnetization under zero-field-cooled (ZFC), field-cooled (FC) and field-warming (FW) are measured with  $\mu_0 H = 0.01$ T, both in parallel and perpendicular to the

$c$  axis, as seen in Fig. 1(d). A ferromagnetic transition is clearly observed approximately 150K for both direction, similar to the literatures<sup>23,27,28</sup>. The ZFC and FC curves show obvious splitting in  $\mathbf{H}//c$  below  $T_C$  like other typical frustrated ferromagnets<sup>11,29,30</sup>, and the difference in magnitude for the two direction indicates the anisotropic character of the low temperature magnetic phase. A slight kink at  $\sim 125\text{K}$  below  $T_C$  was also observed, consistent with the possible two-stage magnetic ordering transition<sup>26</sup>. The magnetization curve at  $T = 5\text{K}$  for both  $\mathbf{H}//c$  and  $\mathbf{H}//ab$  direction distinctly demonstrates the strong magneto-crystalline anisotropy in  $\text{Fe}_3\text{GeTe}_2$  with the easy axis along the  $c$  direction. The saturated magnetic moment ( $M_s$ ) is  $3.25 \mu_B/\text{f.u.}$  for  $\mathbf{H}//c$ , also consistent with the reported values<sup>21,23,31</sup>.

The magneto-transport properties for  $\mathbf{H}$  perpendicular to the current plane have been previously investigated<sup>6,31</sup>, and a large anomalous Hall current has been identified in the  $ab$  plane owing to the topological nodal line band structure<sup>6</sup>. In this work, firstly we measured  $\rho_{xy}$  and  $\rho_{xx}$  in the  $ab$  plane by gradually rotating the  $\mathbf{H}$ , from the usual  $c$ -axis to the  $ab$  plane, as shown in the middle scheme of Fig. 2. We define the angle between the external magnetic field and the normal of the sample plane as  $\theta$ . When  $\theta = 0^\circ$ , a large anomalous Hall resistivity and Hall angle are reproduced in our samples and shown in supplementary Fig. S1, consistent with previously reported<sup>6</sup>. With  $\theta$  increasing from  $0^\circ$  to  $90^\circ$  continuously, we find that  $\rho_{xy}$  gradually reduces, while a pronounced cusp-like anomaly observed in the low field region of the curve, as shown in Fig. 2(a). It becomes most distinct for  $\theta = 90^\circ$ , that is  $\mathbf{H}//\mathbf{I}$ , therefore the name of PTHE is given. At this configuration, the contribution of the AHE is almost completely excluded. Simultaneously, clear bend appeared in the MR curves in Fig. 2(b), indicating some undefined transitions in the magnetization progress.

In the meantime, the full angular dependence from  $0$ - $360^\circ$  of  $\rho_{xy}$  and MR in this case are also investigated, as shown in Figs. 2(c, d). In a normal situation, the curve is expected to follow a rough  $\cos\theta$  relation, as the AHE scaled with the out-of-plane component of  $\mathbf{H}$ <sup>32</sup>. While the AHE component at  $\theta = 90$  or  $270^\circ$  is expected to vanish, there remained small value in the figure, which are caused by the misalignment error. It is noted here only at  $\mu_0 H = 3\text{T}$  that the curve accords with a good  $\cos\theta$  relation, while at  $\mu_0 H = 0.5\text{T}$  and  $1\text{T}$ , on account of the existence of the large PTHE, it deviates and presents a sharp sign-reverse across the  $90$  or  $270^\circ$ . Therefore, the PTHE can always be detected in the configuration of  $\mathbf{H} //$  current plane, as observed in our other samples in

supplementary Fig. S2, with magnitude in similar scale. The MR showed two-fold pattern peaking around  $90^\circ$  ( $270^\circ$ ), with anisotropy of  $\sim -0.5\%$  ( $= (\rho_{\parallel} - \rho_{\perp})/\rho_{\perp}$ ) under a field of 3T.

Furthermore, to establish a clearer picture of this abnormal PTHE, we measured the in-plane Hall resistivity  $\rho_{xy}$  and MR at various temperatures from 5K to 170 K when  $\mathbf{H} // \mathbf{I}$ , as shown in Figs. 3(a, b). The cusp in  $\rho_{xy}$  was being highest at  $T=100\text{K}$  and persisted all temperatures below  $T_C$  in the low field region. The MR curves are all negative while bend or upturn emerges at lower temperature. Here the in-plane Hall data was disposed in the same process as that in normal mutual-vertical configuration. The PTHE contribution is denoted as  $\rho_{xy}^{\text{PT}}$ , thus the total Hall resistivity is:  $\rho_{xy} = \mu_0 R_0 H + R_S M + \rho_{xy}^{\text{PT}}$ , where the first two terms represent the ordinary and anomalous Hall contribution, respectively. As the MR is overall less than 1%,  $R_S$  can usually be simplified as  $S_A \rho_{xx}^2$ , in which  $S_A$  is field independent and  $\rho_{xx}$  is the longitudinal resistivity<sup>33,34</sup>.  $\rho_{xy}^{\text{PT}}$  is thus extracted in combination with the in-plane M-H curves, as showed representatively in Fig. 3(c), which also demonstrated that the peak of  $\rho_{xy}$  just appears at the anisotropy field of the M-H curve. By extracting  $\rho_{xy}^{\text{PT}}$  over the temperature range of 5-170 K, we constitute the phase diagram in Fig. 3(d), by contour mapping in the temperature and magnetic field plane. In general, the PTHE exists from 0.3T to 1.5T, and covers the whole temperature below  $T_C$ . A maximum value of  $2.04 \mu\Omega \cdot \text{cm}$  is obtained at 100K in  $\text{Fe}_3\text{GeTe}_2$  single crystal, which is quite large and nearly more than ten times of those observed in systems containing skyrmion phases, such as  $\text{MnGe}$ <sup>35</sup> ( $\sim 0.16 \mu\Omega \cdot \text{cm}$ ),  $\text{Mn}_3\text{Ga}$ <sup>36</sup> ( $\sim 0.26 \mu\Omega \cdot \text{cm}$ ) and  $\text{MnNiGa}$ <sup>11</sup> ( $\sim 0.15 \mu\Omega \cdot \text{cm}$ ).

Finally, we measured the angular dependence of  $\rho_{xy}$  and MR with the field rotated in the  $ab$  plane at 100K to examine the in-plane anisotropy. The angle between  $\mathbf{H}$  and  $\mathbf{I}$  in the  $ab$  plane is denoted as  $\varphi$ . It can be seen in Figs. 4(a, b) that the PTHE can be altered substantially by the change of  $\varphi$ , while the MR shows slight increase with similar shape. By sweeping in the positive (+H) and negative field (-H), we obtain two curves of  $\rho_{xy}(\varphi)$  which are actually not superposed, demonstrating again the existence of large antisymmetric PTHE. The angular dependence of  $\rho_{xy}$  extracted by  $(\rho_{xy}(+H) - \rho_{xy}(-H))/2$ , as shown in the inset of Fig. 4(a), is well-described by the  $\sin \varphi$  formulation. Largest magnitude is presented at  $H=1\text{T}$ , where the PTHE dominates. But it should be noted that the evolution of planar  $\rho_{xy}$  with  $\varphi$  is not fixed. Our measurements of several samples present varying tendency upon  $\varphi$  changing, while they all follow a rough  $\sin(\varphi + x)$  relation (supplementary Fig. S3). Therefore, the largest PTHE is not always observed at  $\mathbf{H} // \mathbf{I}$ , like

in the concerned sample here. Presently we can only attribute the discrepancy to the different state of the surface of our samples, where further investigation is still needed. The so-called PHE, which is obtained by the regular procedure of  $(\rho_{xy}(+H) + \rho_{xy}(-H))/2$ , is shown in Fig. 4(c). Similar to the reported behavior<sup>18,32</sup>, it roughly followed  $\rho_{xy}^{\text{PHE}} = (\rho_{\parallel} - \rho_{\perp}) \sin \varphi \cos \varphi$ , where  $\rho_{\parallel}$  and  $\rho_{\perp}$  are the resistivity when  $\mathbf{H}$  applied parallel or perpendicular to  $\mathbf{I}$ . Hence the variation of  $\rho_{xy}^{\text{PHE}}$  depends on AMR (expressed as  $(\rho_{\parallel} - \rho_{\perp})/\rho_{\perp}$ )<sup>37</sup>. Both the magnitude of PHE and AMR is rather small, implying the weak in-plane anisotropy of this van der Waals ferromagnet.

Moreover, from the expression of  $\rho_{xy}^{\text{PHE}}$ , it can be seen that planar  $\rho_{xy}^{\text{PHE}}$  will vanish when  $\mathbf{I}$  is perpendicular or parallel to  $\mathbf{H}$  ( $\varphi = 0$  or  $\pi/2$ ), and will exhibit symmetric relationship to  $\mathbf{H}$  instead of antisymmetric one like a conventional Hall effect<sup>15, 18</sup>. There are some examples where AHE-like signal is observed<sup>19,20</sup>, which are currently explained by either a high-order contribution or non-collinear spin structure. But PTHE is a novel phenomenon that first identified. We presumed that a gauge field  $\mathbf{h}$ , pointed in the out-of-plane direction, as shown in the schematic picture in Fig. 4(a), should emerge to give an extra enhancement of  $\rho_{xy}$  in the low field region. One possible origin is the suspected topological (bubble-like) domain structure in the  $ab$  plane of  $\text{Fe}_3\text{GeTe}_2$  proposed by the previous MFM and STM measurements<sup>38, 39</sup>. Notably, the observed PTHE nearly completely exclude the contribution from AHE, resulting in a pure examination of THE, which can be a potential detection method of in-plane skyrmion formation<sup>40</sup>. The other supposition is the spin chirality induced by non-collinear spin structure. During the in-plane magnetization process, the spins of Fe atoms would rotate from the easy  $c$  axis to the  $ab$  plane, during which a noncoplanar spin structure might appears, leading to the non-vanishing spin chirality.

## Conclusion

In summary, by three dimensional rotation of the magnetic field with respect to the sample plane, we have observed a large planar topological Hall effect in the hard-magnetized but easily-cleavable  $ab$  plane in van der Waals ferromagnet  $\text{Fe}_3\text{GeTe}_2$ . Systematic studies on the angular dependence revealed the dynamical evolution of the Hall resistivity and MR which are invariantly measured in the  $ab$  plane. The PTHE exists in the whole temperature region below  $T_c$  and reaches the maximum value of  $2.04 \mu\Omega \cdot \text{cm}$  at 1.2T at 100K, which is much larger than those observed in other skyrmion systems. We attribute the origin of this large PTHE to the emergence of a gauge field, which is either

generated by the possible topological domain structure of uniaxial Fe<sub>3</sub>GeTe<sub>2</sub> or the non-coplanar spin structure formed in the process of in-plane magnetization. It should be mentioned that, during the submission of this manuscript, the skyrmion crystal in the *ab* plane is reported by T. E. Park *et al*<sup>41</sup>, which strongly support one of our presumptions. Therefore, PTHE can be a prominent way to detect in-plane skyrmion formation, practically in the natural two-dimensional system and thin films, where the Hall effect on other sides are hardly accessible.

## Acknowledgement

This work is supported by National Natural Science Foundation of China (11604148, 51601092), the National Key R&D Program of China (Grant No. 2017YFA0303202), and the Key Research Program of the Chinese Academy of Sciences, KJZD-SW-M01.

## References

- [1] N. Nagaosa, and Y. Tokura, Emergent electromagnetism in solids. *Phys. Scripta* **2012**, 014020 (2012).
- [2] H. Chen *et al.*, Anomalous Hall effect arising from noncollinear antiferromagnetism. *Phys. Rev. Lett.* **112**, 017205 (2014).
- [3] S. Nakatsuji *et al.*, Large anomalous Hall effect in a non-collinear antiferromagnet at room temperature. *Nature* **527**, 212 (2015).
- [4] A. K. Nayak *et al.*, Large anomalous Hall effect driven by a nonvanishing Berry curvature in the noncollinear antiferromagnet Mn<sub>3</sub>Ge. *Sci. Adv.* **2**, e1501870 (2016).
- [5] E. Liu *et al.*, Giant anomalous Hall effect in a ferromagnetic Kagome-lattice semimetal. *Nat. Phys.* **14**, 1125 (2018).
- [6] Kim, K. *et al.*, Large anomalous Hall current induced by topological nodal lines in a ferromagnetic van der Waals semimetal. *Nat. Mater.* **17**, 794 (2018).
- [7] Y. Taguchi *et al.*, Spin chirality, Berry phase, and anomalous Hall effect in a frustrated ferromagnet. *Science* **291**, 2573 (2001).
- [8] Y. Machida *et al.*, Unconventional anomalous Hall effect enhanced by a noncoplanar spin texture in the frustrated Kondo lattice Pr<sub>2</sub>Ir<sub>2</sub>O<sub>7</sub>. *Phys. Rev. Lett.* **98**, 057203 (2007).
- [9] N. Kanazawa *et al.* Large Topological Hall Effect in a Short-Period Helimagnet MnGe. *Phys. Rev. Lett.* **106**, 156603 (2011).
- [10] S. X. Huang, and C. L. Chien. Extended Skyrmion Phase in Epitaxial FeGe(111) Thin Films.

- Phys. Rev. Lett. **108**, 267201 (2012).
- [11] W. Wang *et al.*, A Centrosymmetric Hexagonal Magnet with Superstable Biskyrmion Magnetic Nanodomains in a Wide Temperature Range of 100-340 K. *Adv. Mater.* **28**, 6887 (2016).
- [12] J. P. Pan, in *Solid State Physics*, edited by F. Seitz and D. Turnbull (Academic, New York, 1957), Vol. 5, pp. 1–96.
- [13] Z. Q. Lu *et al.*, Planar Hall effect in NiFe/NiMn bilayers. *J. Appl. Phys.* **90**, 1414 (2001).
- [14] K. M. Seemann, *et al.*, Origin of the planar Hall effect in nanocrystalline  $\text{Co}_{60}\text{Fe}_{20}\text{B}_{20}$ . *Phys. Rev. Lett.* **107**, 086603 (2011).
- [15] H. X. Tang *et al.*, Giant planar Hall effect in epitaxial (Ga,Mn) as devices. *Phys. Rev. Lett.* **90**, 107201 (2003).
- [16] A. A. Burkov, Giant planar Hall effect in topological metals. *Phys. Rev. B* **96**, 041110 (2017).
- [17] S. Nandy *et al.*, Chiral anomaly as the origin of the planar Hall effect in Weyl semimetals. *Phys. Rev. Lett.* **119**, 176804 (2017).
- [18] H. Li *et al.*, Giant anisotropic magnetoresistance and planar Hall effect in the Dirac semimetal  $\text{Cd}_3\text{As}_2$ . *Phys. Rev. B* **97**, 201110 (2018).
- [19] P. K. Muduli *et al.*, Antisymmetric contribution to the planar Hall effect of  $\text{Fe}_3\text{Si}$  films grown on GaAs(113)A substrates. *Phys. Rev. B* **72**, 104430 (2005).
- [20] Y. You *et al.*, Anomalous Hall effect–like behavior with in-plane magnetic field in noncollinear antiferromagnetic  $\text{Mn}_3\text{Sn}$  films. *Adv. Electron. Mater.* **5**, 1800818 (2019).
- [21] H. J. Deiseroth *et al.*,  $\text{Fe}_3\text{GeTe}_2$  and  $\text{Ni}_3\text{GeTe}_2$ —two new layered transition-metal compounds: crystal structures, HRTEM investigations, and magnetic and electrical properties. *Eur. J. Inorg. Chem.* **2006**, 1561 (2006).
- [22] Y. Wang *et al.*, Anisotropic anomalous Hall effect in triangular itinerant ferromagnet  $\text{Fe}_3\text{GeTe}_2$ . *Phys. Rev. B* **96**, 134428 (2017).
- [23] A. F. May *et al.*, Magnetic structure and phase stability of the van der Waals bonded ferromagnet  $\text{Fe}_{3-x}\text{GeTe}_2$ . *Phys. Rev. B* **93**, 014411 (2016).
- [24] B. Chen *et al.*, Magnetic properties of layered itinerant electron ferromagnet  $\text{Fe}_3\text{GeTe}_2$ . *J. Phys. Soc. Jpn.* **82**, 124711 (2013).
- [25] V. Y. Verchenko *et al.*, Ferromagnetic order, strong magnetocrystalline anisotropy, and magnetocaloric effect in the layered telluride  $\text{Fe}_{3-\delta}\text{GeTe}_2$ . *Inorg. Chem.* **54**, 8598 (2015).
- [26] J. Yi *et al.*, Competing antiferromagnetism in a quasi-2D itinerant ferromagnet:  $\text{Fe}_3\text{GeTe}_2$ . *2D Mater.* **4**, 011005 (2016).
- [27] Y. Liu *et al.*, Anomalous Hall effect in the van der Waals bonded ferromagnet  $\text{Fe}_{3-x}\text{GeTe}_2$ . *Phys. Rev. B* **97**, 165415 (2018).
- [28] Y. Liu *et al.*, Critical behavior of the van der Waals bonded ferromagnet  $\text{Fe}_{3-x}\text{GeTe}_2$ . *Phys. Rev.*

- B **96**, 144429 (2017).
- [29] Z. Hou *et al.*, Observation of various and spontaneous magnetic skyrmionic bubbles at room temperature in a frustrated kagome magnet with uniaxial magnetic anisotropy. *Adv. Mater.* **29**, 1701144 (2017).
- [30] Z. Hou *et al.*, Manipulating the Topology of Nanoscale Skyrmion Bubbles by Spatially Geometric Confinement. *ACS Nano*, **13**, 922 (2019).
- [31] Y. Wang *et al.*, Anisotropic anomalous Hall effect in triangular itinerant ferromagnet  $\text{Fe}_3\text{GeTe}_2$ . *Phys. Rev. B* **96**, 134428 (2017).
- [32] N. Kumar *et al.*, Planar Hall effect in the Weyl semimetal GdPtBi. *Phys. Rev. B* **98**, 041103 (2018).
- [33] S. X. Huang, and C. L. Chien, Extended Skyrmion phase in epitaxial FeGe(111) thin films. *Phys. Rev. Lett.* **108**, 267201 (2012).
- [34] Y. Li *et al.*, Robust formation of Skyrmions and topological Hall effect anomaly in epitaxial thin films of MnSi. *Phys. Rev. Lett.* **110**, 117202 (2013).
- [35] N. Kanazawa *et al.*, Large topological Hall effect in a short-period helimagnet MnGe. *Phys. Rev. Lett.* **106**, 156603 (2011).
- [36] P. Sergelius *et al.*, Berry phase and band structure analysis of the Weyl semimetal NbP. *Sci. Rep.* **6**, 33859 (2016).
- [37] D. Thompson *et al.*, Thin film magnetoresistors in memory, storage, and related applications. *IEEE T. Magn.* **11**, 1039 (1975).
- [38] N. León-Brito *et al.*, Magnetic microstructure and magnetic properties of uniaxial itinerant ferromagnet  $\text{Fe}_3\text{GeTe}_2$ . *J. Appl. Phys.* **120**, 083903 (2016).
- [39] G. D. Nguyen *et al.*, Visualization and manipulation of magnetic domains in the quasi-two-dimensional material  $\text{Fe}_3\text{GeTe}_2$ . *Phys. Rev. B* **97**, 014425 (2018).
- [40] T. Yokouchi *et al.*, Formation of In-plane Skyrmions in Epitaxial MnSi Thin Films as Revealed by Planar Hall Effect. *J. Phys. Soc. Jpn.* **84**, 104708 (2015).
- [41] T. E. Park *et al.*, arxiv: 1907.01425.

## Figures and captions

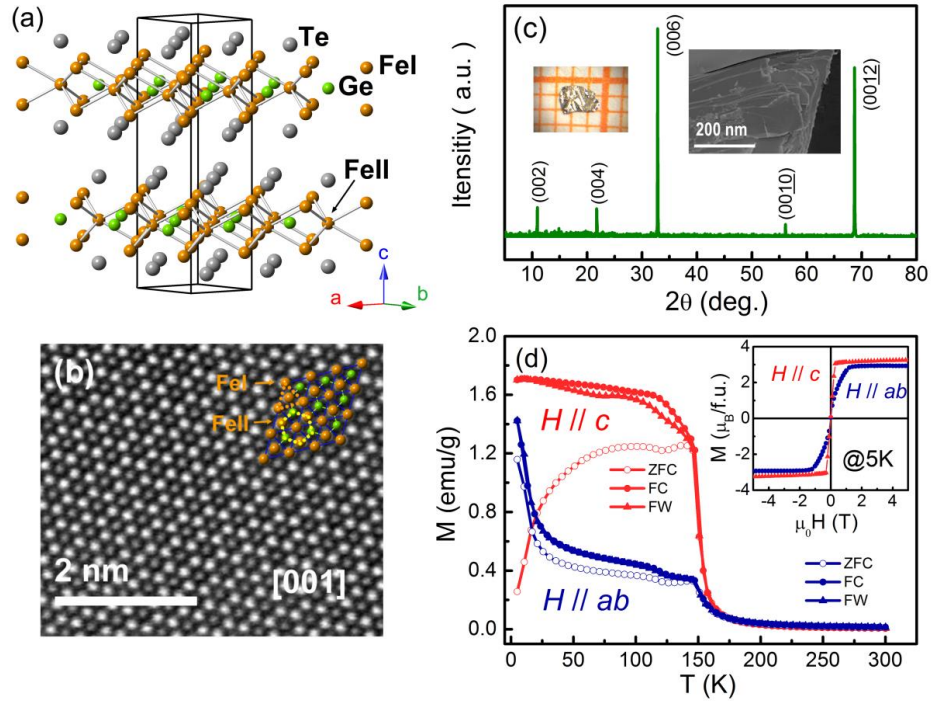


FIG. 1. Structure and magnetic properties of the single crystal  $\text{Fe}_3\text{GeTe}_2$ . (a) Schematic of the hexagonal structure of  $\text{Fe}_3\text{GeTe}_2$  (space group  $P6_3/mmc$ ). (b) High-resolution STEM image taken on the  $[001]$  axis. The inset shows the arrangement of triangular lattice structure of FeI atoms and the hexagonal atomic ring of FeII-Ge layer. (c) XRD pattern for  $\text{Fe}_3\text{GeTe}_2$  single crystal. Inset shows the optical photograph (left) and SEM image (right) of an as-grown slice  $\text{Fe}_3\text{GeTe}_2$  single crystal. (d) Temperature dependence of the ZFC, FC and FW magnetization measured at  $\mu_0 H = 0.01\text{T}$  for  $\mathbf{H} // ab$  and  $\mathbf{H} // c$ . The inset shows the anisotropic M-H curve at  $T = 5\text{K}$ .

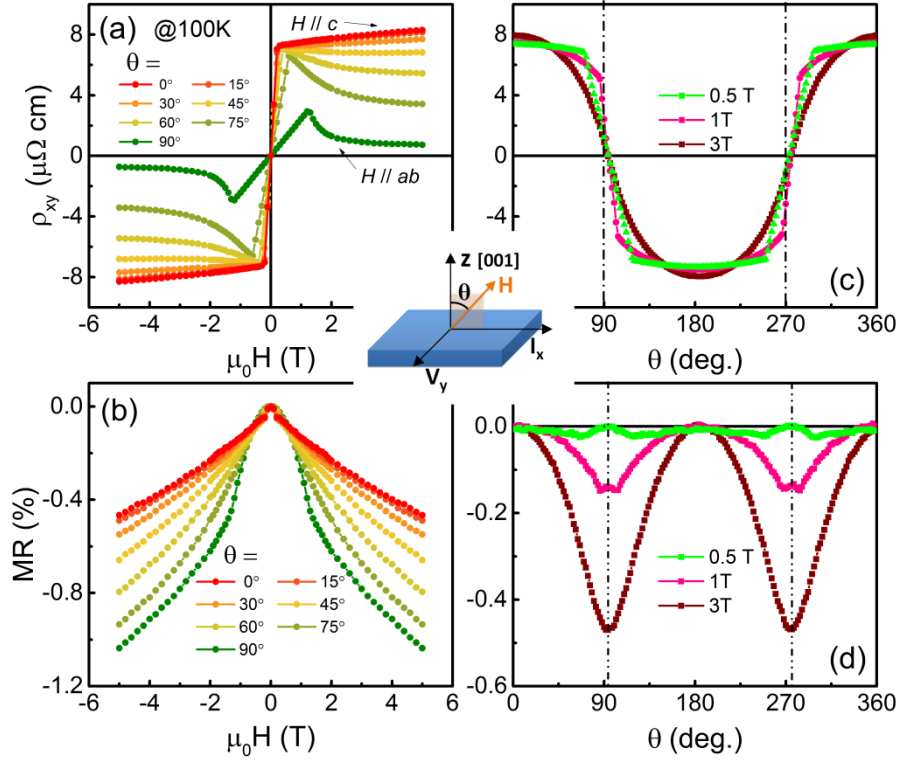


FIG. 2. Separate (a)  $\rho_{xy}(H)$  and (b) MR curves measured in the  $ab$  plane with  $\mathbf{H}$  direction of  $\theta = 0^\circ, 15^\circ, 30^\circ, 45^\circ, 60^\circ, 75^\circ$  and  $90^\circ$  at 100K. The angular dependence of (c)  $\rho_{xy}$  and (d) MR at 100K under the field of 0.5T, 1T and 3T. In the middle it shows the schematic of the measurement configuration.

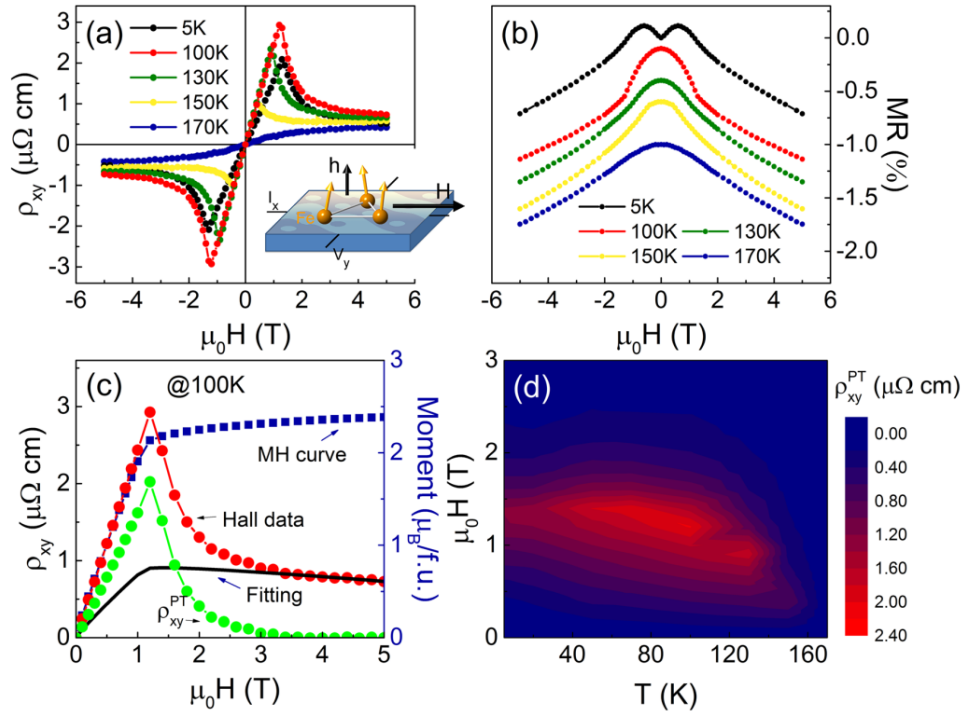


FIG. 3. In-plane (a)  $\rho_{xy}$  and (b) MR of Fe<sub>3</sub>GeTe<sub>2</sub> single crystal at various temperatures for  $\mathbf{H} // \mathbf{I}$ . Inset is the configuration of the measurement, as well as schematic of the possible origin that generated an inside gauge field of  $\mathbf{h}$ . (c) The representative  $\rho_{xy}$  curve (red) and MH curve (blue) measured at 100K, calculated  $R_0 B + S_A \rho_{xx}^2 M$  fitting curve (black) and extracted  $\rho_{xy}^{PT}$  curve (green). (d) The contour mapping of extracted  $\rho_{xy}^{PT}$  as a function of the external magnetic field and temperature.

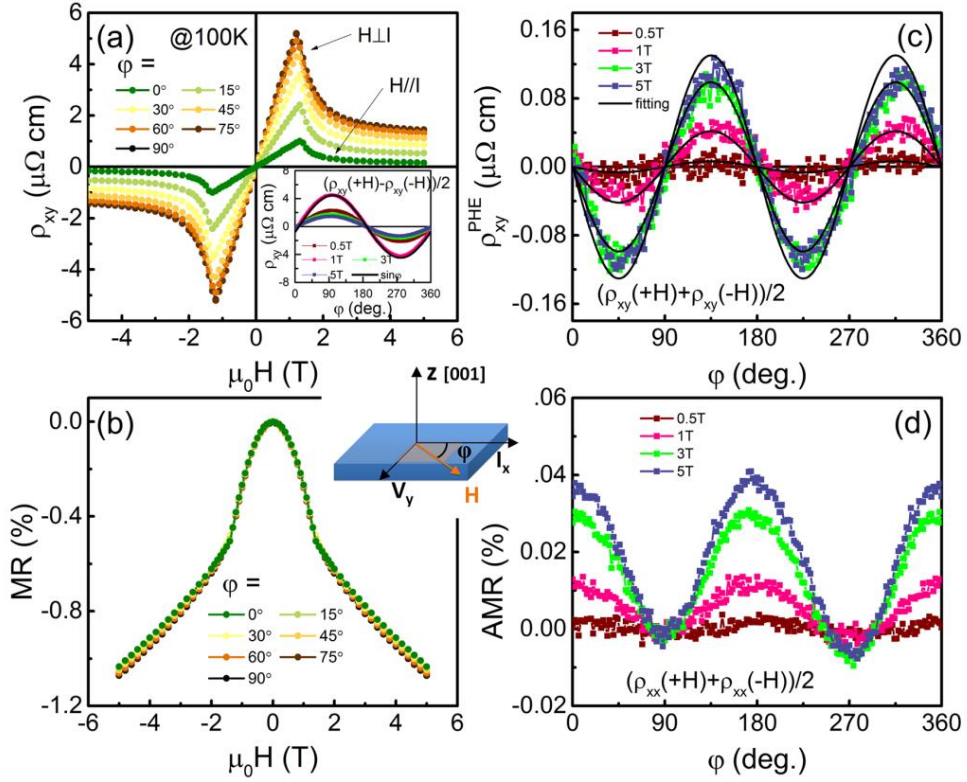


FIG. 4. Magnetic field dependence of planar (a)  $\rho_{xy}$  and (b) MR at  $\varphi = 0^\circ, 15^\circ, 30^\circ, 45^\circ, 60^\circ, 75^\circ$  and  $90^\circ$  at 100K. The inset in (a) is the angular dependence of  $\rho_{xy}$  by subtracting the original curve in positive and negative field  $((\rho_{xy}(+H) - \rho_{xy}(-H))/2)$ . The angular dependence of the (c)  $\rho_{xy}^{PHE}$ , obtained by  $(\rho_{xy}(+H) + \rho_{xy}(-H))/2$  and (d) AMR at 100K under the field of 0.5T, 1T, 3T and 5T.

## Supplementary Materials

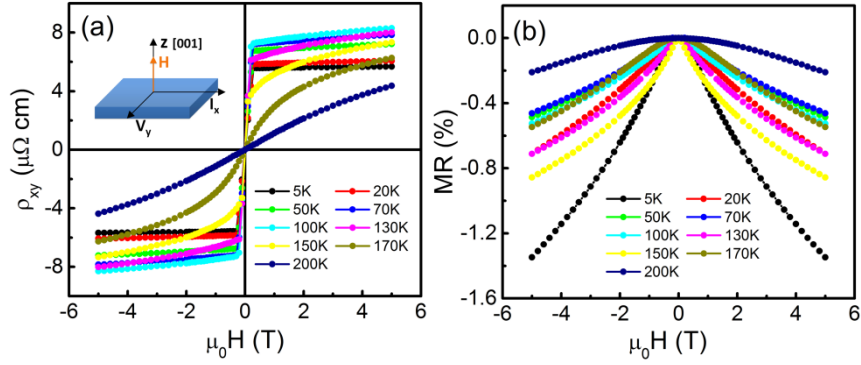


FIG. S1. Magnetic field dependence of (a) Hall resistivity  $\rho_{xy}$  and (b) MR for  $\mathbf{H} // \mathbf{c}$  at various temperature of the same sample as measured in Fig. 2 and Fig. 3.

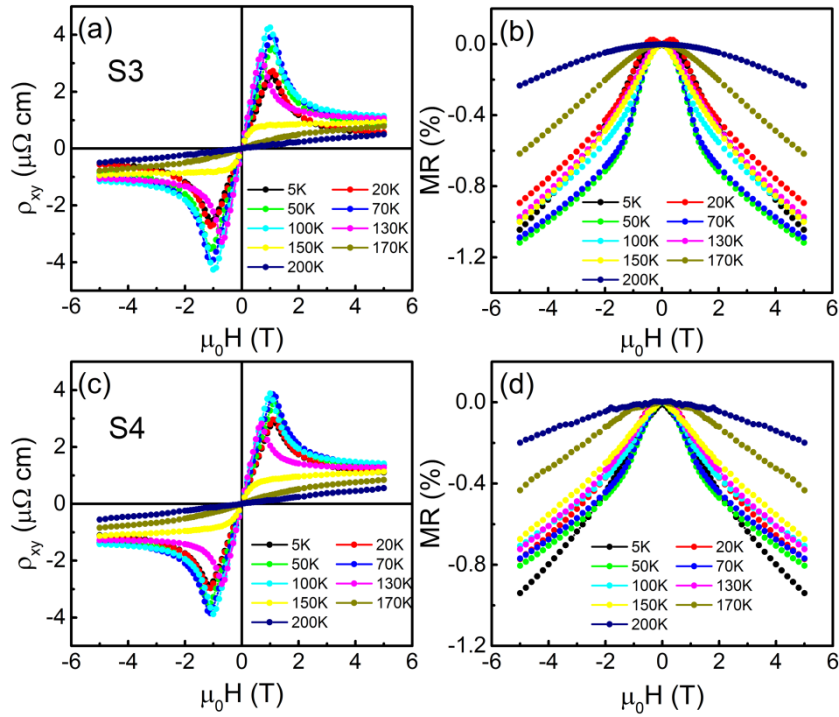


FIG. S2. Magnetic field dependence of (a, c) Hall resistivity  $\rho_{xy}$  and (b, d) MR with  $\mathbf{H} // \mathbf{I}$  at various temperature for another two samples labeled as S3 and S4.

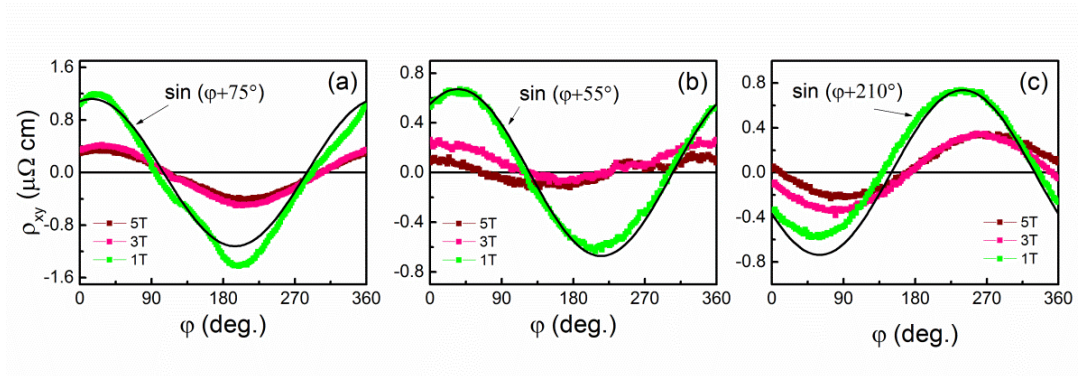


FIG. S3. Angular dependence of  $\rho_{xy}$  by subtracting the original curve in positive and negative field  $((\rho_{xy}(+H) - \rho_{xy}(-H))/2)$  of three other samples (S5-S7) at 100K under the field of 1T, 3T and 5T.